JOURNAL OF EXPERIMENTAL AND THEORETICAL PHYSICS, 2024, Vol. 165, No. 3, pp. 334–353

ATOMS, MOLECULES, OPTICS

POLARIZATION CHARACTERISTICS OF ELECTRODYNAMIC STARK EFFECT SPECTRA

© 2024 A.V. Demura [a*], D.S. Leontyev [a], V.S. Lisitsa [a,b,c]

[a] National Research Centre Kurchatov institute 123182, Moscow, Russia
[b] National Research University MPTI 141701, Dolgoprudny, Moscow region, Russia
[c] National Research Nuclear University MEPI 115409, Moscow, Russia

*e-mail: demura45@gmail.com

Received October 27, 2023
Revised November 15, 2023
Accepted November 15, 2023

Abstract. The detailed study of physical processes responsible for the hydrogen atom spectra under its motion transverse to the strong magnetic field – due to electrodynamic Stark effect, known also as MSE (Motional Stark Effect) – is performed. The formation mechanisms of excited hydrogen levels population due to collisions with protons of plasma are investigated. The experimental and theoretical data on the total and partial excitation cross sections along with parabolic quantum numbers in the laboratory frame of moving atom are confronted. The universal approach for the calculations of cross sections in the basis of the parabolic wave functions with an account of their adiabatic suppression in the low energy range of collisions and selective in terms of the parabolic quantum numbers is proposed. The method developed is applied for the construction of the collisional-radiative kinetic model for the partial populations of the excited Stark sublevels calculations taking into account the ionization due to collisions with protons. The sources of the thermodynamically nonequilibrium origin of the Stark sublevel populations in the electrodynamic Stark effect are revealed in the wide diapason of the plasma density variation. The intensities of π- and σ Stark components of H_α line versus beam energy, magnetic field and plasma density are calculated. The polarization characteristics of MSE spectra of H_α line are calculated in the magnetically confined thermonuclear plasma. The obtained results are in the reasonable agreement with the literature data. The developed method is of interest as from the general physical point of view, as for the MSE-spectroscopy of tokamaks and in the other experimental conditions.

Keywords: *Motional Stark Effect*, *polarization characteristics of H-atom spectra*, *Balmer alpha line*, *tokamak plasma*, *parabolic wave functions*

DOI: 10.31857/S00444510240304e2

1. INTRODUCTION

The observation of the electrodynamic Stark effect or MSE (Motional Stark Effect) is used for diagnostic purposes when probing plasma with a beam of neutral hydrogen across the magnetic field B. At the same time, registration and analysis of the polarization characteristics of the emission spectrum formed in an electric field

$$\mathbf{F} = \frac{\mathbf{v} \times \mathbf{B}}{c},$$

arising in the coordinate system of an atom moving at a velocity **v** when it intersects magnetic fields lines provide information on the magnitude and distribution of magnetic fields and associated currents [1-7], where c is the speed of light. Indeed, the spectrum of a hydrogen atom in a stationary homogeneous electric field **F** consists of Stark π-components polarized along **F** and a σ-components with polarization across **F**, the splitting of which is proportional to the magnitude of the electric field [1, 2]. As a result, in the absence of isotropy for the real geometry of a plasma installation, for example, a tokamak, it is possible to isolate and analyze the polarized components of the observed emission spectrum [1-20]. Experimental implementations of the technique are local and have a fairly good spatial

resolution [1-20]. In the case of a tokamak, it can be used to identify the slope profile of the magnetic field line $\gamma_p(r) = \text{arctg}(B_p(r) / B_t)$ (where $\mathbf{B}_t$ is toroidal, and $\mathbf{B}_p$ is the poloidal magnetic fields associated with the discharge current, r is the magnitude of a small radius, measured from the position of the magnetic axis of the plasma in the toroidal discharge chamber) by determining the local deviations of the vector $\mathbf{B}$ from the initial vector of the toroidal field $\mathbf{B}_t$ by a small angle [1–7]. Knowledge of the magnetic field line slope profile, in turn, allows to establish the spatial distributions of the absolute values of the discharge parameters, for example, the cord stability factor, the discharge current, and to estimate the profile of current density in the tokamak discharge [1–7].

An extensive literature is devoted to the problem of MSE diagnostics, which discusses both the theoretical foundations of the MSE method [1-20] and its implementation and interpretation in experiment [1-20]. However, both of these problems are very complex and challenging. In the present work, only the theoretical aspects of this problem are considered.

To use MSE diagnostics in an experiment, it is assumed to measure the intensity and polarization of radiation from beam atoms in plasma. To do this, it is necessary to know the populations of the Stark sublevels. This implies solving the problem of atomic kinetics of Stark states. To solve the kinetic problem of the Stark levels, it requires rate coefficients of collisional and radiative processes based on parabolic wave functions of a hydrogen atom, which include a description of excitation, deexcitation, radiative decay and ionization in collisions with protons and electrons of plasma, with account of transitions between levels with different principal quantum number n and between sublevels of the same n. The specifics of this kinetic problem consists in the necessity to use a Stark (parabolic) basis, whereas previously such data were calculated only in the basis of spherical wave functions averaged over magnetic quantum numbers involved in the interaction of atomic levels [11, 17-20]. In the next step, the populations of Stark states are used to calculate the radiation spectrum and determine its polarization characteristics for the purposes of MSE diagnostics. The output data are influenced not only by the choice of the basis of wave functions, but also by the methods and approximations used to calculate the cross sections of processes and their rate coefficients in the absence of thermodynamic equilibrium and in the presence of an external electric field of an electrodynamic nature.

In contrast to the previously obtained results, in this work, the parabolic basis of wave functions and Born cross sections of collision processes with a normalized probability of corresponding transitions are used at all stages of the calculation. The deviation from the Born approximation in the region of low velocities is taken into account by the introduction of an adiabatic factor arising from the solution of two level system within strong coupling method [21]. A detailed comparison with the literature data [11, 22-24] demonstrates the high efficiency and reliability of the proposed approach and the results obtained.

2. STARK SUBLEVELS EXCITATION CROSS SECTIONS CALCULATION IN HYDROGEN-LIKE ION PARABOLIC BASIS WAVE FUNCTIONS

2.1. General provisions

The observed radiation spectrum of the Stark level structure, formed when a beam of fast atoms moves across a magnetic field, is formed by atomic processes that determine the population of the upper levels of individual Stark components. The excitation of the Stark sublevels (components) is determined mainly by collisions with fast protons moving at superthermal velocity in the atomic rest frame. The characteristic velocities of neutrals of the diagnostic beams [11, 17-20], and therefore in proton-atomic collisions, are comparable or slightly exceed the typical values of the atomic velocities of electrons in the first Bohr orbit, corresponding to proton energies of the order of 25 keV. From the point of view of atomic collision physics, this velocity range is intermediate between fast (Born limit) and slow (adiabatic limit) collisions. The adiabaticity parameter, determined by the ratio of the transition frequency between the upper and lower levels to the collision rate, differs greatly for transitions from the ground state and between excited levels. For transitions from the ground state, consideration of the adiabatic factor is essential, whereas for transitions between excited levels it can be neglected if the energy difference between the corresponding levels is small, for example, for transitions between states with the same principal quantum number n.

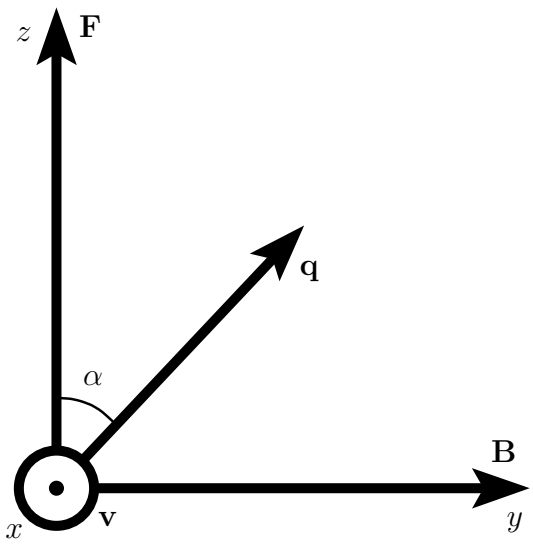

Fig. 1. MSE Vector Scheme

When considering inelastic collisions of heavy particles — hydrogen atoms with protons — the momentum of a fast particle practically does not change [25], and the effective transmitted momentum **q** is relatively small and with good accuracy is almost perpendicular to the momentum of the incident particle [25]. To calculate the effective excitation cross sections of hydrogen atom transitions in collisions with protons, parabolic wave functions are used in the work. The consideration is divided into three cases: 1) excitation from the ground state; 2) transitions between excited states; 3) transitions between Stark sublevels inside a given level with the principal quantum number n.

Fig. 1 shows a the relative directions in the beam lab frame: **q** is the transmitted momentum, which lies in the same plane with the induced electric field **F** and forms an arbitrary angle with it; **B** is the vector of the magnetic field, **v** is the velocity of plasma ions, which collide with diagnostic beam neutrals in the lab frame. This velocity is equal in magnitude to the velocity of the beam **V** and has the opposite direction.

The calculation of effective collision cross sections was carried out in the first Born approximation [24, 25] (atomic units):

$$\sigma(\upsilon) = 2\pi \int_{q_{min}}^{q_{max}} \frac{dq}{q^3} W(q), \qquad (1)$$
$$q_{min} = \frac{\Delta E}{\upsilon}, \quad q_{max} = 2\upsilon,$$

where ΔE is the energy difference between the levels, $W(q)$ is the probability of transition, determined by the formula

$$W(q) = \int_0^{2\pi} \frac{d\alpha}{2\pi} W(\alpha, q), \quad W(\alpha, q) = \frac{4\left|R(\alpha, q)\right|^2}{\upsilon^2}, \qquad (2)$$

$R(\alpha, q)$ is the matrix element of the transition [25]. In the parabolic basis (taking into account the chosen geometry of the problem), it has the form

$$R(\alpha, q) = \left\langle n'k'm' \mid e^{i\mathbf{q}\cdot\mathbf{r}} \mid nkm \right\rangle = \int_0^{\infty} d\xi \int_0^{\infty} d\eta \frac{\xi + \eta}{4} \int_0^{2\pi} \frac{d\varphi}{2\pi} \Psi^*_{n'k'm'}(\xi, \eta, \varphi) \times \exp\left\{ iq \left(\frac{\xi - \eta}{2} \cos\alpha + \sqrt{\xi\eta} \sin\alpha \sin\varphi \right) \right\} \times \Psi_{nkm}(\xi, \eta, \varphi), \qquad (3)$$

where n, k, m and n', k', m' are the principal, electric and magnetic quantum numbers of the initial and final states correspondingly; Ψ_{nkm} and $\Psi_{n'k'm'}$ are the parabolic wave functions of the initial and final states, respectively; ξ, η are parabolic coordinates, φ is azimuth angle.

Using the integral representation of the Bessel function of the first kind with an integer order s [26],

$$J_s(x) = \frac{1}{2\pi} \int_{-\pi}^{\pi} \exp\left\{ -is\tau + x \sin\tau d\tau \right\},$$

one could integrate (3) by azimuth angle φ:

$$\int_0^{2\pi} \frac{d\varphi}{2\pi} \exp\left\{ i\Delta m\varphi + q\sqrt{\xi\eta} \sin\alpha \sin\varphi \right\} = e^{i\Delta m\pi} \int_{-\pi}^{\pi} \frac{d\varphi'}{2\pi} \exp\left\{ -i\Delta m\varphi' + iq\sqrt{\xi\eta} \sin\alpha \sin\varphi' \right\} = (-1)^{\Delta m} J_{\Delta m}(x), \qquad (4)$$
$$\varphi = \pi - \varphi', \quad \Delta m + m - m', \quad x = q\sqrt{\xi\eta} \sin\alpha.$$

Then the expression for the matrix element takes the form

$$R(\alpha,q)=(-1)^{\Delta m}\int_0^\infty d\xi\int_0^\infty d\eta\frac{\xi+\eta}{4}\times$$
$$\times\Psi^*_{n',k',m'}(\xi,\eta)\exp\left\{iq\frac{\xi-\eta}{2}\cos\alpha\right\}\Psi_{n,k,m}(\xi,\eta)\times \quad (5)$$
$$\times J_{\Delta m}(q\sqrt{\xi\eta}\sin\alpha),$$

where $\Psi_{n,k,m}(\xi,\eta)$ and $\Psi_{n',k',m'}(\xi,\eta)$ are the coordinate parts of the parabolic wave functions. To avoid confusion, it should be pointed out that the labeling of wave functions using the electric quantum number k is done for brevity and simplification of writing, since these functions are the product of two wave functions depending on different variables and parabolic quantum numbers n_1 and n_2, respectively, and $k = n_1 - n_2$ [25, 27]. And, it is in terms of parabolic quantum numbers n_1, n_2, the real calculations of matrix elements are carried out [25].

2.2. Generalized Born approximation with normalized probability and adiabatic factor

As is known, the conditions of applicability of the first Born approximation can be violated if the value for the transition probability turns out to be greater than one [28, 29]. It is customary to eliminate this disadvantage by introducing forced normalization of the expression for the transition probability in the Born approximation [28, 29], for which it is necessary to solve transcendental equations at each step of integration, when representing the effective collision cross section as an integral over the impact parameter ρ [28,29]. However, due to the equivalence of the quasiclassical and wave considerations of the Born approximation [30], the normalization in this paper is achieved by a new simpler method – introducing a branching factor over the transmitted momentum q. In this case, the normalized probability has the form

$$W_{norm}(q)=\frac{W(q)}{1+W(q)}. \quad (6)$$

In addition, at low energies, the standard Born approximation is not valid which leads, as is known, to a sharp increase of cross sections in the region of low velocities [21, 25, 28, 29]. The correct description of slow collisions is a difficult problem associated with solving the problem of strong coupling of atomic states, which, however, radically depends on the number of levels taken into account. In this paper, this problem is solved on the basis of the strong coupling method for two-level system [20], which takes into account a strong pairwise coupling between the ground and excited states. This method allows to move to low velocities by multiplying the expression $W(q)$ by an additional adiabatic factor. The adiabatic factor is determined by an exponent in the power equal to the ratio of the transition frequency $\omega = \Delta E/\hbar$ to the inverse collision time

$$\tau_{col}^{-1}=\frac{\upsilon}{\rho_W}\sim\frac{\upsilon^2}{n^2}$$

with a minus sign [21], where ρ_W is the Weisskopf radius.

In this case, the normalized probability is determined by

$$W_{norm}(q)=\frac{W(q)\exp\{-\frac{\Delta En^2}{\upsilon^2}\}}{1+W(q)\exp\{-\frac{\Delta En^2}{\upsilon^2}\}}. \quad (7)$$

Further substitution of (6) and (7) in (1) makes it possible to obtain normalized effective excitation cross sections with correct behavior in the region of low collision energies.

The analysis of available literature data [11, 22-24] shows that even for the hydrogen atom, the results of calculations of excitation cross sections by different methods differ greatly both from each other and in comparison with the experiment [22]. Figure 2 shows the results of calculations of the excitation cross sections of the $n = 3$ level from the ground state in the first Born approximation [24, 25] (hereinafter referred to as the Born method for short), the strong coupling method [23] and the Glauber method [11, 31, 32]. The cross sections shown in the figure (curves 4-6) are the sum of the partial cross sections

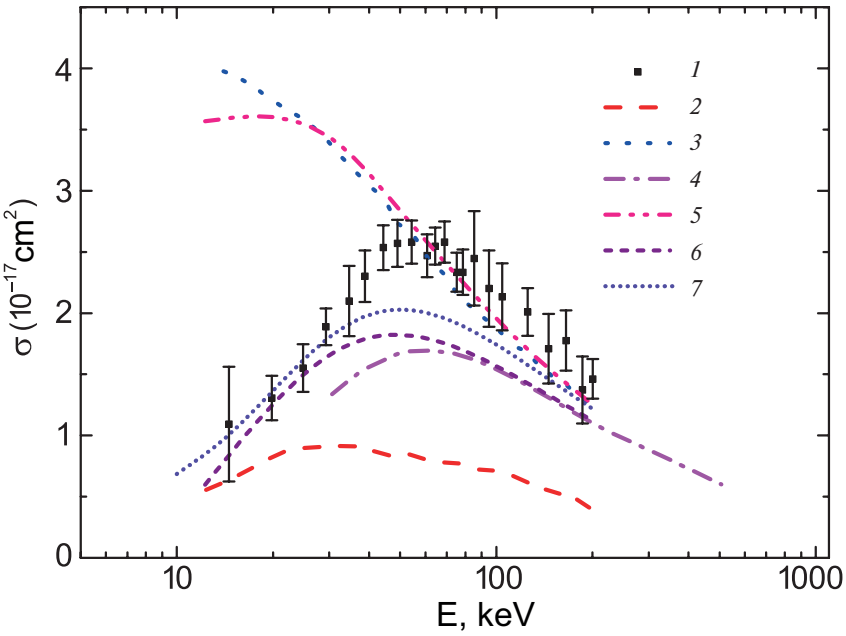

Fig. 2. The total excitation cross section of level with $n = 3$ from the ground state: *1* — experiment [22]; *2* — strong coupling model, taking into account 7 states [23]; *3* — Born method [24]; *4* — Glauber method [11]; *5* — Born method with probability normalization (6); *6* — the Born method with a probability normalization and an adiabatic factor (7); *7* — calculation using the approximation formula [33]

of the excitation of the transition over the parabolic quantum numbers *km*. It follows from the presented comparison that the total cross section calculated in the Born approximation in a parabolic basis according to formula (6) coincides with the same total cross section calculated in spherical coordinates [24]. This condition must be fulfilled for general reasons [25] and is an indicator of the accuracy of the calculations performed. In the range of low energies, calculations performed by the Born method with normalization of probability and account of the adiabatic factor (7) and the Glauber method [11] agree better with the experiment. At high energies, both the Born method and the Glauber method show a fairly good agreement with experimental data [11]. At the same time, the total cross section calculated in the strong coupling model [23] with account of 7 states, lies much lower than the rest ones.

It should be noted that the calculations in [11] were carried out in the basis of spherical wave functions (WF) $n'l'm'$, account of in the collision frame and using their transformation by rotation into WF nlm, defined in the coordinate system associated with the electric field, followed by the expression of parabolic WF via the specified WF nlm. Such a cumbersome transformation leads to the appearance of terms in the expression for effective cross sections due to interference of scattering amplitudes, and significantly complicates the analysis and obtaining results.

To construct a kinetic collisional-radiative model, calculations of the partial excitation cross sections using parabolic quantum numbers are necessary. Figures 3 and 4 present a comparison of partial excitation cross sections of the ground state calculated by the Born method with probability normalization (6) and account of the adiabatic factor (7). It can be seen that with account of the adiabatic factor in the region of low energies, the excitation cross sections decrease, and at high energy the cross sections approach the Born limit.

In addition to the effective partial excitation cross sections of the ground state, numerical calculations of the partial cross sections of transitions between excited *nkm* levels with different principal quantum numbers, as well as transitions without changing the principal quantum number, were performed for the analysis of atomic kinetics within the framework of the same approach. As functions of energy, these cross sections behave to some extent similar to the dependencies described above, but show a strong variation in values for different specific *nkm* of upper and lower levels, which can reach several orders of magnitude. In this case, for example, the cross sections of transitions between states with the principal quantum numbers differing by 1 can be either

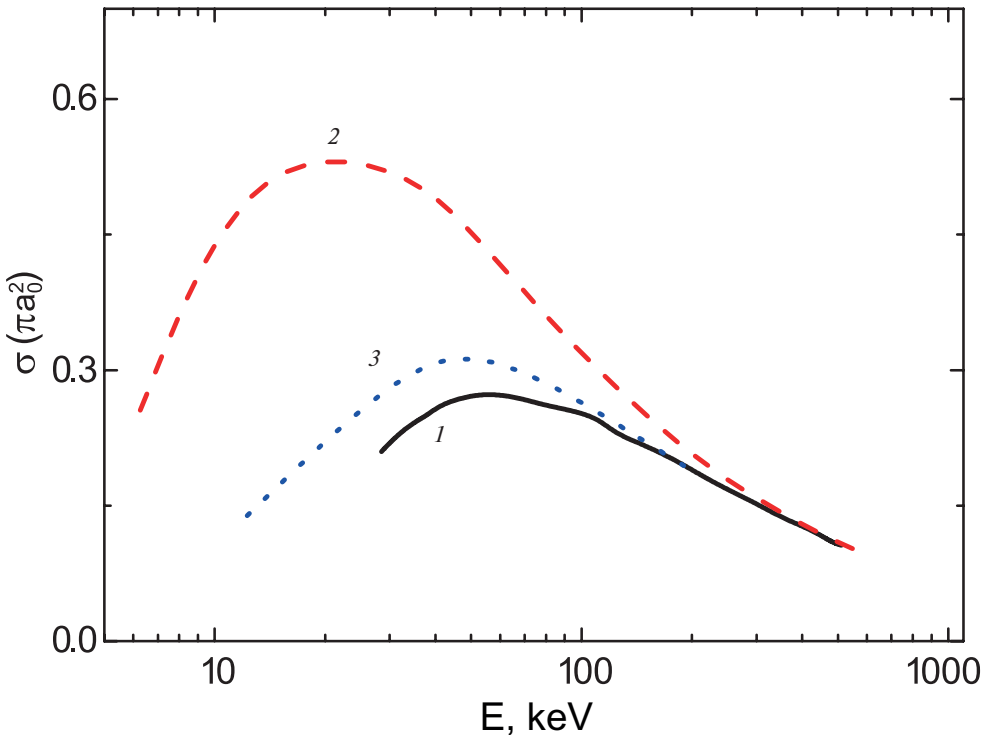

Fig. 3. Effective cross section of transition 100 → 210: : *1* — Glauber method [11]; *2* — Born method with probability normalization (6); *3* — Born's method with probability normalization and adiabatic factor (7)

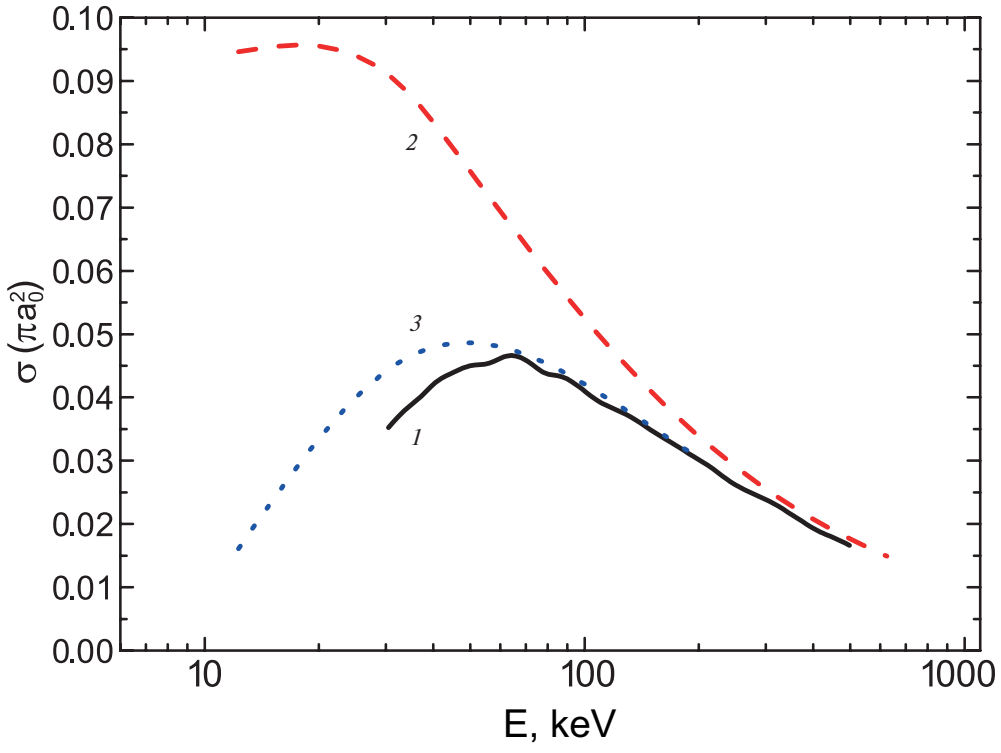

Fig. 4. Effective cross section of transition 100 → 320 : *1* — Glauber method [11]; *2* — Born method with probability normalization (6); *3* — Born method with probability normalization and adiabatic factor (7)

of the same order with cross sections without changing n, or differ from them by several orders of magnitude. Therefore, the lack of results of such cross sections calculations in the literature and the irregularity of their values greatly complicate the analysis of atomic kinetics in the *nkm* representation.

3. COLLISIONAL-RADIATIVE KINETICS OF STARK SUBLEVELS POPULATION

Based on the data on collisional-radiative processes calculated in the basis of parabolic wave functions, a kinetic model was constructed to determine the populations of all states of the hydrogen atom in the range of the principal quantum numbers n = 1- 6. The rates of radiative decays were calculated using the Gordon formulas [27]. The excitation and deexcitation cross sections in collisions with protons were calculated in accordance with the procedure described in section 2. A system of 56 linear algebraic equations was solved, which determines the population of Stark sublevels N_a:

$$-N_a\left[N_p\sum_b g_b \upsilon\sigma_{ab}(\upsilon) + A_a^{Tot} + N_p\sigma_a^{ion}(\upsilon)\right] + \\ +\sum_{b\neq a} N_b\left[A_{ba} + g_a N_p \upsilon\sigma_{ba}(\upsilon)\right] = 0,$$

$$A_a^{Tot} = \sum_{b<a} A_{ab}, \quad a,b = 1-56, \tag{8}$$

where a, b are sets of quantum numbers *nkm* of the corresponding state, g_a, g_b are the statistical weights of the states, A_{ab} is the probability of radiative decay, N_p is the plasma density, and $\sigma_a^{ion}(\upsilon)$ is the ionization cross section of the a level [33, 34]. At the same time, two cases were considered: 1) without ionization due to collisions with protons ($\sigma_{ion}(\upsilon) = 0$); 2) with ionization. Approximation formulas [33, 34] were used for effective integral cross sections of levels ionization with the principal quantum number n, which were obtained by fitting the results of calculations using the Monte Carlo method [35]. Since partial cross sections of collisional ionization of parabolic states are not available in the literature, the total cross sections of proton ionization, given in [33, 34], were used. The kinetic model was limited only to states $n = 1-6$, while the total approximation cross sections from [33,34] were used to describe the kinetics of sublevels with $n = 6$. This choice of basis was established on the statements [17-19] about the small influence of the kinetics of the upper levels with $n \geqslant 5$ on the populations of the Stark sublevels with $n = 3$, which determine the polarization characteristics of the H_α line radiation. In addition, as can be seen from previous calculations [17, 18], at plasma

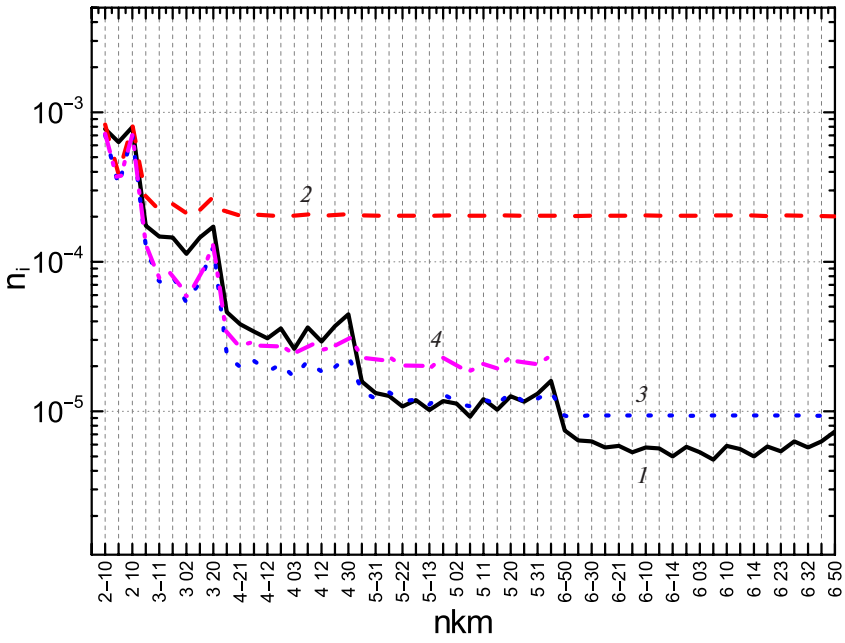

Fig. 5. Calculated relative populations of $n_i = N_i / g_i$ of Stark sublevels $i = nkm$, divided by statistical weight at $B = 3$ T, $N_p = 3 \cdot 10^{13}$ cm^{-3}, $E = 50$ keV: *1* – data from [17]; *2* – kinetic model with account of of proton ionization (states $n = 1-6$); *3* — kinetic model, taking into account proton ionization (states $n = 1-6$); *4* — kinetic model with account of proton ionization (states $n = 1-5$)

density of ~ 10^{13} cm^{-3}, the populations of states decrease sharply in magnitude with increase of n, and the absolute amplitude of population jumps of different km states within one n becomes very small, therefore, the use of a roughened approach in the form of total proton ionization cross sections looks quite justified in the context of the stated goals. In addition, under the assumption of stationarity, an additional condition is the equality of the sum of the relative populations of all levels to 1. Figure 5 shows the calculated level populations at the magnetic field value $B = 3$ T, beam energy $E = 50$ keV and plasma density $N_p = 3 \cdot 10^{13}$ cm^{-3}.

A comparison with the data from [17] reveals a relatively satisfactory agreement of population distributions in the range $n = 1– 6$, if we take into account that in [17] the kinetic scheme included levels with $n = 1–10$ and the system of nonstationary kinetics was solved with account of collisional ionization and charge exchange on a neutral beam, as well as electron-atomic collisions [11]. In [17], the Glauber method was used to calculate excitation cross sections using spherical wave functions nlm, followed by a transition to parabolic quantum numbers. The comparison demonstrates the significant influence of proton ionization on the distribution of populations of the upper levels, and to a lesser extent on the distribution of populations of the lower levels with $n = 2 – 3$. In addition, the influence of the number of states included has also been demonstrated. It is shown that the populations of states $n = 3 – 5$, obtained in the kinetic model with $n = 1– 6$, lie below the populations obtained with $n = 1– 5$. At the same time, for level states with $n = 3$ this difference is relatively small. It is also seen that the results of this work reproduce the shape of the population distribution from [17], since it also used the cross sections of ionization in collisions with protons and charge exchange from [33], which do not depend on the electric k and magnetic m quantum numbers were used there also. The existing differences may also be related to the fact that in our kinetic model the contribution of collisions with electrons compared to protons was ignored.

In [17], the population was also calculated taking into account ionization by an induced (electrodynamic) electric field, but this channel does not significantly affect the population of levels with $n = 2–6$. Indeed, calculations using the semi-empirical formula [36] show that the rate of ionization by the field at $E = 100$ keV and $B = 5$ T is negligible for levels with $n = 5$, and for $n = 6$ by 8-10 orders of magnitude is lower than other decay channels – radiative, due to excitation, deexcitation and proton

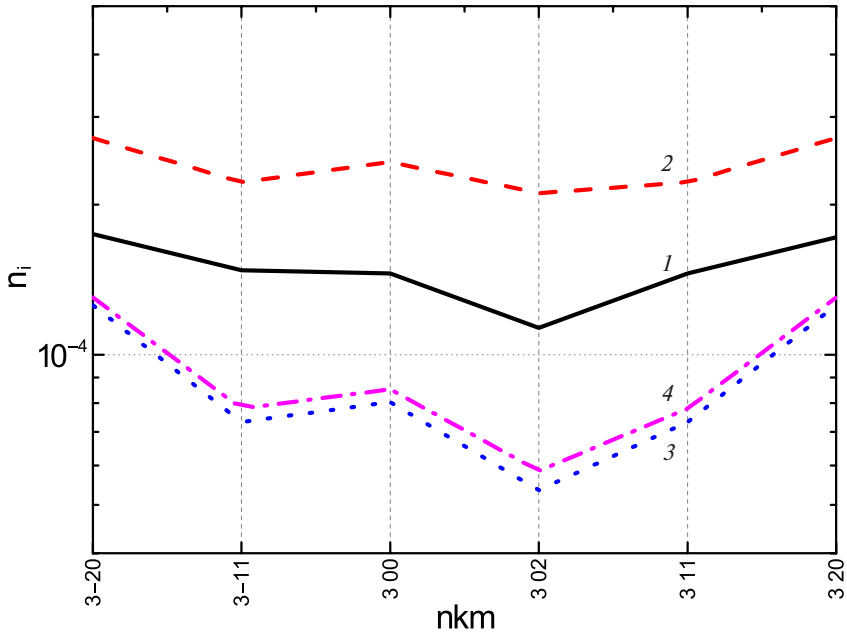

Fig. 6. The calculated relative populations of the upper Stark sublevels of the H_α line, divided by the statistical weight $n_i = N_i / g_i$ at $B = 3$ T, $N_p = 3 \cdot 10^{13}$ cm^{-3}, $E = 50$ keV. *1* — data from [17]; *2* — kinetic model without account of proton ionization (states $n = 1–6$); *3* — kinetic model with account of proton ionization (states $n = 1–6$); *4* — kinetic model with account of proton ionization (states $n = 1–5$)

ionization. This decay channel should need to be included if kinetic calculations also would cover levels with $n \geqslant 8$.

Fig. 6 shows the calculated relative populations of the upper Stark sublevels of the H_α line components. As can be seen from this comparison, the populations in the model with $n = 1$–5 differ little from the case of $n = 1$–6. This is in accordance with the comparison of the calculation results with $n = 1$–10 in [17] and with $n = 1$–5 in [19]. At the same time, the influence of the ionization by protons channel is very significant, while in the cited works with which the comparison was carried out, this was not noted or analyzed in any way.

Indeed, as the analysis shows, the average deviation in percentages of the present calculations of the values for the system of levels $n = 1$–6 and the conditions in Fig. 6 from the data [17] without account of ionization by protons is about 1840%, with account of ionization about 39%, and for $n = 3$ about 62–42%.

It was rightly pointed out in [8, 11, 17-20] that the populations of the Stark sublevels of the atoms of a diagnostic beam should be nonequilibrium — non-thermodynamic, however, the results of kinetic calculations were not analyzed in any way for the nature of this nonequilibrium. The comparison of the rate coefficients obtained in the present work for the conditions presented in Fig. 5 shows that the rates of excitation by protons and the rates of transitions between excited levels significantly exceed the radiative rates, which corresponds to the conditions of the statistical character of the Stark sublevels populations. On the other hand, due to the small energy difference between quantum states in this system compared to the beam energy, all excitation cross sections are approximately the same, which ultimately leads to an equal population of all states (Curve 2 in Fig. 5). At the same time, the ionization rates in collisions with protons at a density of $N_p = 3 \cdot 10^{13}$ cm^{-3} are much higher than the radiative rates, so the populations are ultimately determined by the equilibrium between the excitation and ionization processes. The proton ionization rates increase noticeably as n increases, while the excitation rates are on average approximately constant, which leads to a decrease of populations in this case with an increase of n (see Fig. 5). As it is seen, similar to the data given in [17-20], the population within the fixed principal quantum number decreases slightly with a decrease in the electric quantum number. This is explained by the fact that the excitation cross sections tend to decrease as the magnetic quantum number of the upper sublevel increases.

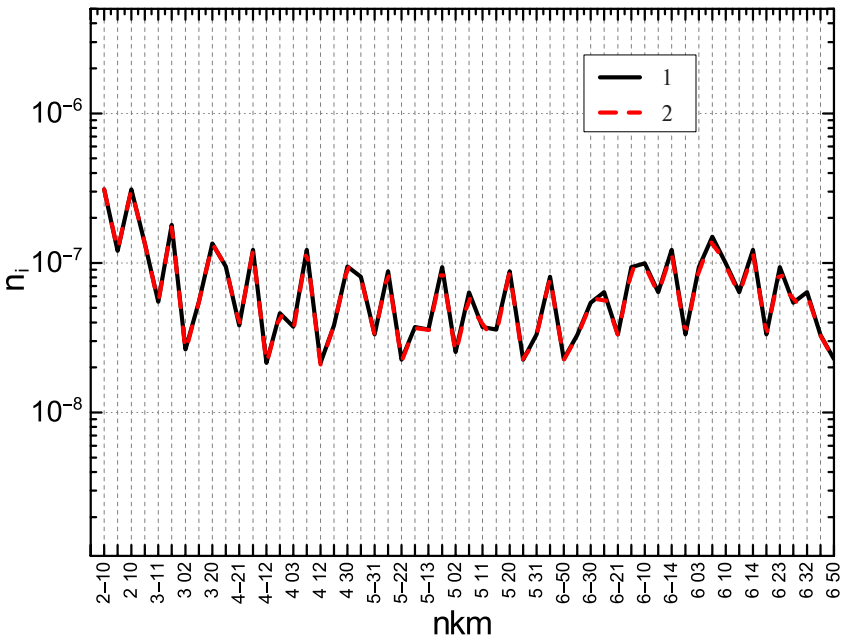

Fig. 7. Calculated relative populations of the Stark sublevels of the line H_α, divided by the statistical weight $n_i = N_i/g_i$ at $B = 3$T, $N_p = 10^{10}$cm^{-3}, $E = 50$ keV. *1* — kinetic model without account of proton ionization (states $n = 1$–6); *2* — kinetic model with account of proton ionization (states $n = 1$–6)

On the other hand, at a low plasma density, one should expect the realization of coronal equilibrium, when populations are determined by the ratio of the excitation rate from the ground state to the total rate of radiative decay decay. Fig. 7 shows the results of calculations of relative populations at beam energy $E = 50$ keV and plasma density $N_p = 10^{10}$ cm^{-3}.

For such a low density, the rate of ionization in collisions with protons already turns out to be less than the radiative rates and does not significantly contribute to the distribution of populations. Since, at the same time, the excitation rates of different levels are still close in magnitude, the distribution of populations depending on nkm acquires the character of peculiar sawtooth fluctuations near a certain average value as the ratio of statistical weights alternates, assuming only two values of 1 or 2 for the Stark sublevels, which, in fact, is shown in Fig. 7. At the same time, despite such non-standard behavior of populations, there is a coronal equilibrium.

4. SYNTHETIC MSE RADIATION SPECTRUM OF H_α LINE

In MSE diagnostics, as a rule, the polarization characteristics of the emission spectrum of the Stark multiplet of the H_α line are analyzed [1–20]. The absolute total intensity I_{3j-2i} of some individual Stark component $3j \to 2i$ of the line H_α is determined by the standard expression

$$I_{3j-2i} = A_{3j-2i}\hbar\omega_{3j-2i}\frac{N_{3j}}{g_{3j}}, \tag{9}$$

where A_{3j-2i} is the probability of radiative decay from sublevel $3j$ to sublevel $2i$, $\hbar\omega_{3j-2i}$ is the energy between the levels, N_{3j}, g_{3j} is the population and statistical weight of the state $3j$ [27], and the numbers in the lower indices are equal to the values of the principal quantum numbers of the corresponding levels. To calculate the intensities of the line components, a stationary system of kinetic equations is solved for the populations of the Stark sublevels of the upper level $3j$ taking into account its connection with other levels. As indicated above, effective cross sections of collisional transitions calculated by the Born method with probability normalization and adiabatic factor (see section 2) are used. In the statistical limit [27] — high density — it is assumed that the levels are populated proportionally to their statistical weight, and the intensity I^{St}_{3j-2i} is determined by the expression

$$I^{St}_{3j-2i} \sim A_{3j-2i}\hbar\omega_{3j-2i}, \tag{10}$$

so the populations of different Stark sublevels are the same! However, as detailed kinetic calculations show that the system plasma + beam of neutrals, with energy much higher than plasma temperature, is nonequilibrium, there is a difference in the populations of the various Stark sublevels even at a very high plasma density.

In the dynamic limit [27] — at low plasma density — the levels populations are determined by the competition between the excitation from the ground state and the total probability of radiative decay A^{Tot}_{3j}, so the $3j$ component intensity in the dynamic limit I^{Dyn}_{3j} for the system of levels $n = 1-6$ is defined by the expression

$$I^{Dyn}_{3j} = A_{3j-2i}\hbar\omega_{3j-2i}\frac{N_p\upsilon}{A^{Tot}_{3j}}\times$$
$$\times\left[\sigma_{1-3j} + \sum_a \frac{A_{4a-3j}\sigma_{1-4a}}{A^{Tot}_{4a}} + \sum_b \frac{A_{5b-3j}\sigma_{1-5b}}{A^{Tot}_{5b}} + \right.$$
$$\left. + \sum_c \frac{A_{6c-3j}\sigma_{1-6c}}{A^{Tot}_{6c}}\right]. \tag{11}$$

Here $\sigma_{1-nj,a,b,c}$ are cross sections of excitation from the ground state to the level with the principal quantum number n and a set of electric and magnetic quantum numbers km (j for $n = 3$, a for $n = 4$, b for $n = 5$, c for $n = 6$) with account of the adiabatic factor, $A_{na,b,c-3j}$ is the probability of radiative decay from level $n = 4,5,6$ to level $3j$, $A^{Tot}_{na,b,c}$ the total probability of radiative decay, N_p plasma density, υ beam velocity.

Figures 8-10 show synthetic spectra of the H_α line with a wavelength of 656 nm corresponding to various plasma and beam parameters. All relative intensities are normalized to the corresponding calculated intensity value of the central component of the line. To understand the relationship between kinetic and statistical distributions of intensities, the scaling factors are given in the insets of corresponding figures in the case of normalization of kinetic

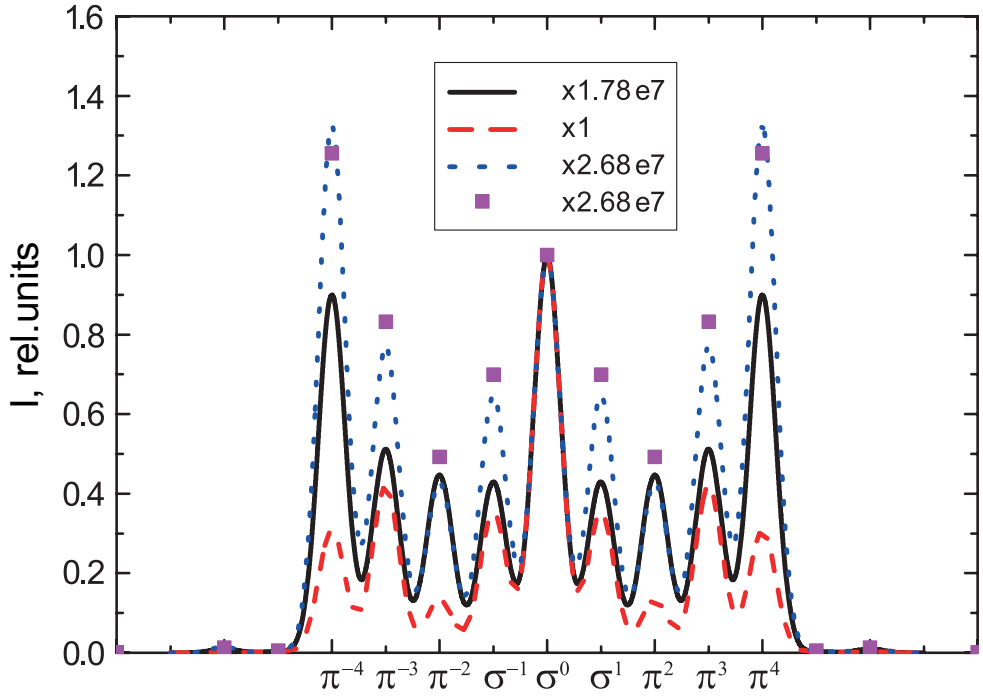

Fig. 8. Synthetic MSE emission spectrum of the H_α line in relative units for $B = 5$ T, $N_p = 10^{10}$ cm^{-3}, $E = 100$ keV: *1* — calculation by the Born method with normalized probability and adiabatic factor (9) with account of ionization; *2* — statistical distribution of populations (10); *3* — distribution of populations in the dynamic limit (11); 4 — calculation from [19] by the Glauber method

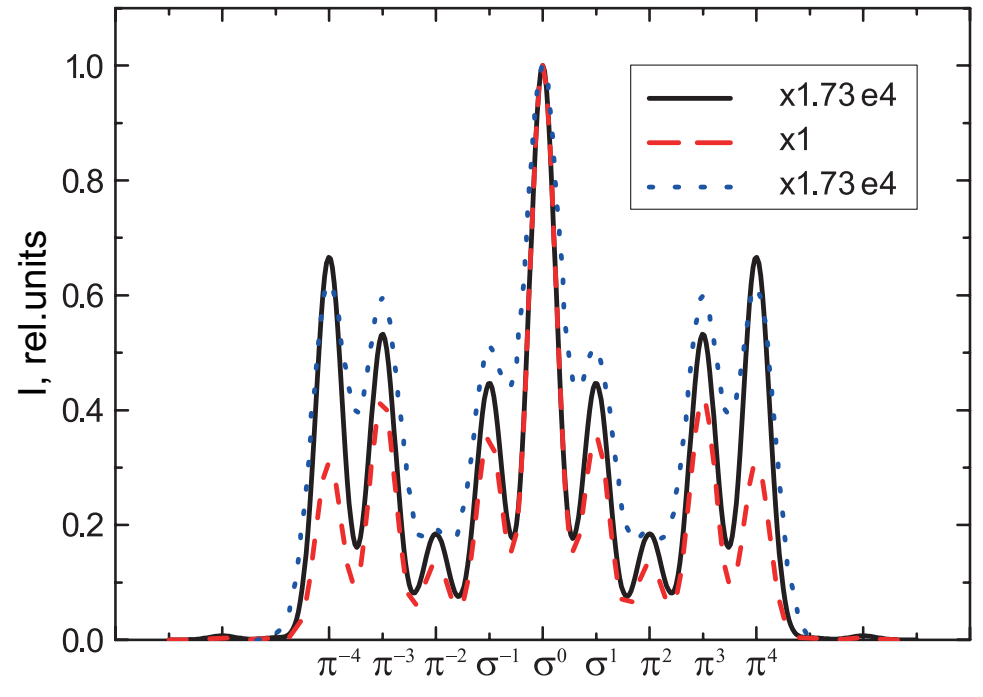

Fig. 9. Synthetic MSE emission spectrum of the H_α line in relative units for $B = 3$ T, $N_p = 10^{13}$ cm^{-3}, $E = 50$ keV: *1* — Born method with normalization of probability and adiabatic factor (9) taking into account ionization; *2* — statistical distribution of populations (10); *3*— calculation from [10] by the Glauber method

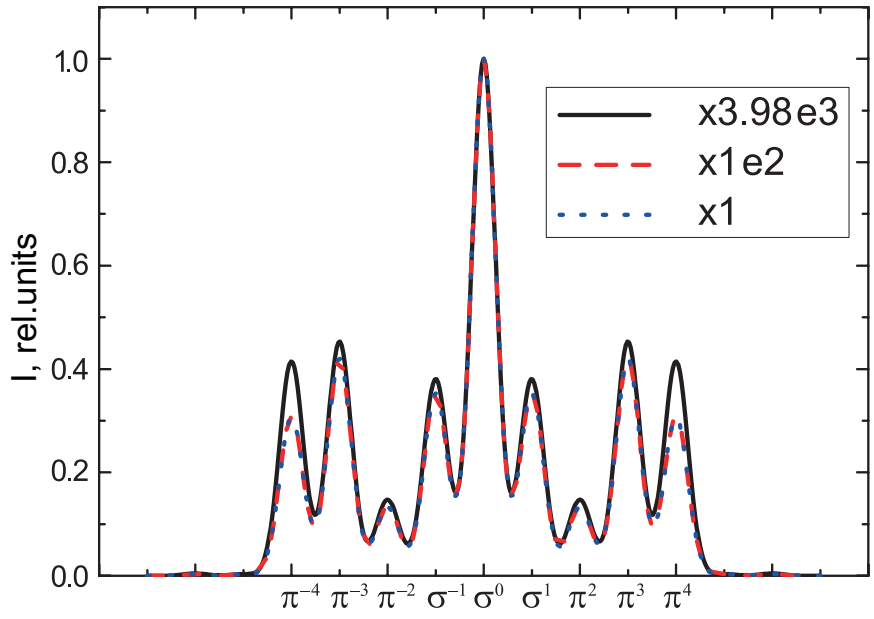

Fig. 10. Synthetic MSE emission spectrum of the line H_α in relative units for $B = 3$ T, $N_p = 10^{16}$ cm^{-3}, $E = 50$ keV: *1* — calculation by the Born method with normalized probability adiabatic factor (9) and with account of ionization; *3* – statistical distribution of populations (10)

distributions by the value of statistical intensity of the central component.

On the abscissa axis, π^d or σ^d designate the relative position of the individual Stark components center in accordance with their polarization (π or σ) and the relative separation $d = (3k_j - 2k_i)$ (in units $(3/2)F$) from the position of the central component of the line. To demonstrate the synthetic spectrum, a Gaussian profile of Stark components with the same half-width $\delta = 0.25$ in the same relative units of the abscissa axis is used in Fig. 8–10. The half-width value was chosen solely for the purpose of visual representation of the line spectrum.

To calculate the populations, a kinetic model was used with account of the hydrogen ionization in collisions with protons [32] under the assumption of observation in the direction perpendicular to beam velocity.

It follows from the comparison of (10) and (11) that static populations are always larger than the dynamic limit and, accordingly, the results of kinetic calculation at low density, but at high density this ratio is not obvious. This is confirmed by the results of calculations of the synthetic H_α spectrum using the kinetic model described above, which are shown in Fig. 8. At the same time, Figures 8-10 are mainly of a demonstrative nature, since the corresponding calculations were performed to reveal the nature of the change in the synthetic spectrum depending on the magnitude of the magnetic field, plasma density and beam energy. For example, for such large magnetic field values as in Fig. 8, it is already necessary to take into account the quadratic Zeeman effect and a simplified MSE description is not applicable here [37].

Figures 8-10 show how the coronal approximation is realized at low plasma density and the statistical limit in dense plasma. As the density increases in Fig. 9, 10, the difference between the statistical intensities and the synthetic ones, calculated with account of proton ionization, decreases. In addition, in Fig. 10 it is noticeable that with account of ionization the intensity ratio deviates from the statistical limit, indicating a change of the equilibrium nature.

The comparison of the relative intensities in Fig. 8-10, normalized to the corresponding value of the intensity of the central component, demonstrates good agreement with the results of other authors.

The results of this analysis show that at both low and high densities, the “kinetic” populations in the neutral energetic beam-plasma system are much smaller than statistical ones and have a nonequilibrium nonthermodynamic character.

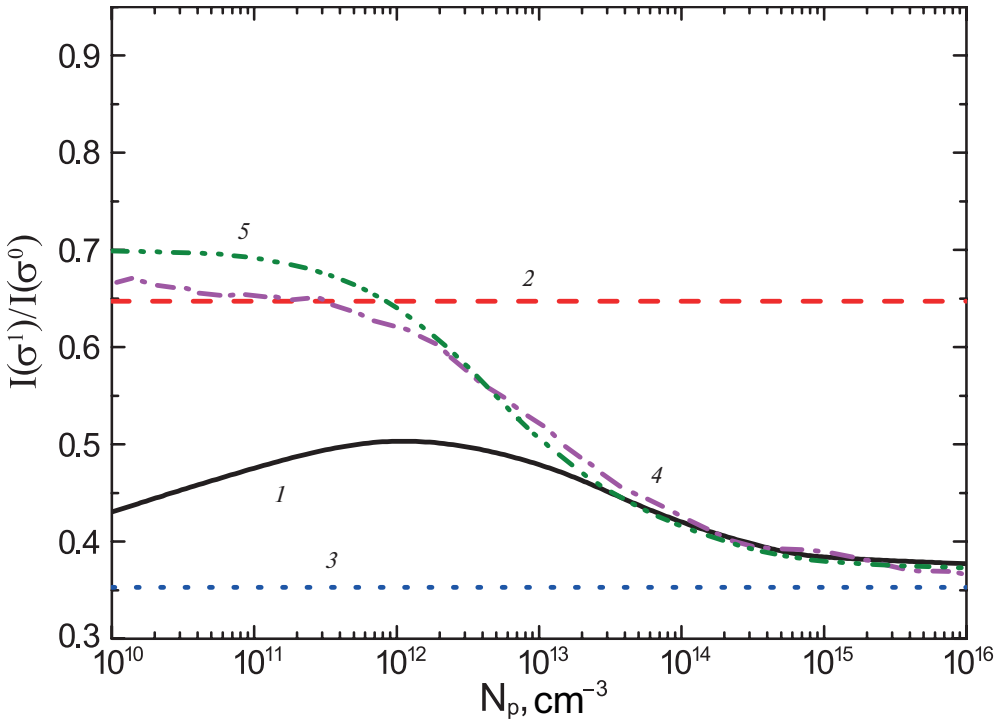

Fig. 11. The ratio of the intensities $I(\sigma^1)$ / $I(\sigma^0)$ of the H_α line depending on the plasma density (B = 5 T, E = 100 keV): *1* — calculated data for (9) with account of ionization; *2* — dynamic limit (11); *3* — statistical limit (10); *4* — data [17]; *5* — data from [19]

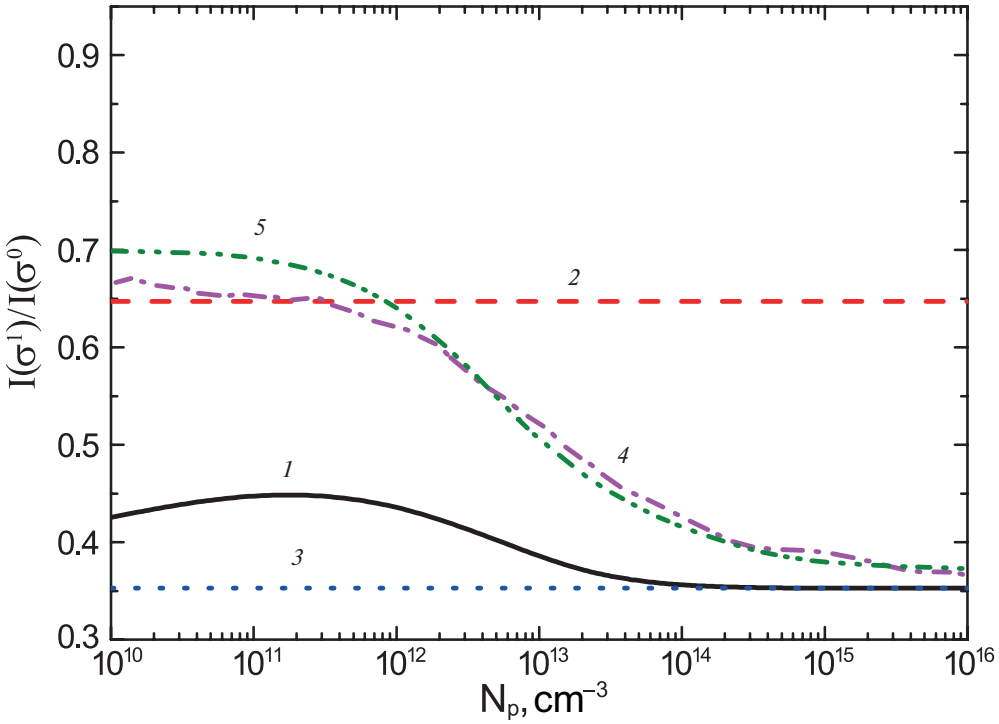

Fig. 12. The ratio of the intensities $I(\sigma^1)$ / $I(\sigma^0)$ of the H_α line depending on the plasma density (B = 5 T, E = 100 keV): *1* — calculated data without (9) account of ionization; *2* — dynamic limit (11); *3* — statistical limit (10); *4* — data [17]; *5* — data from [19]

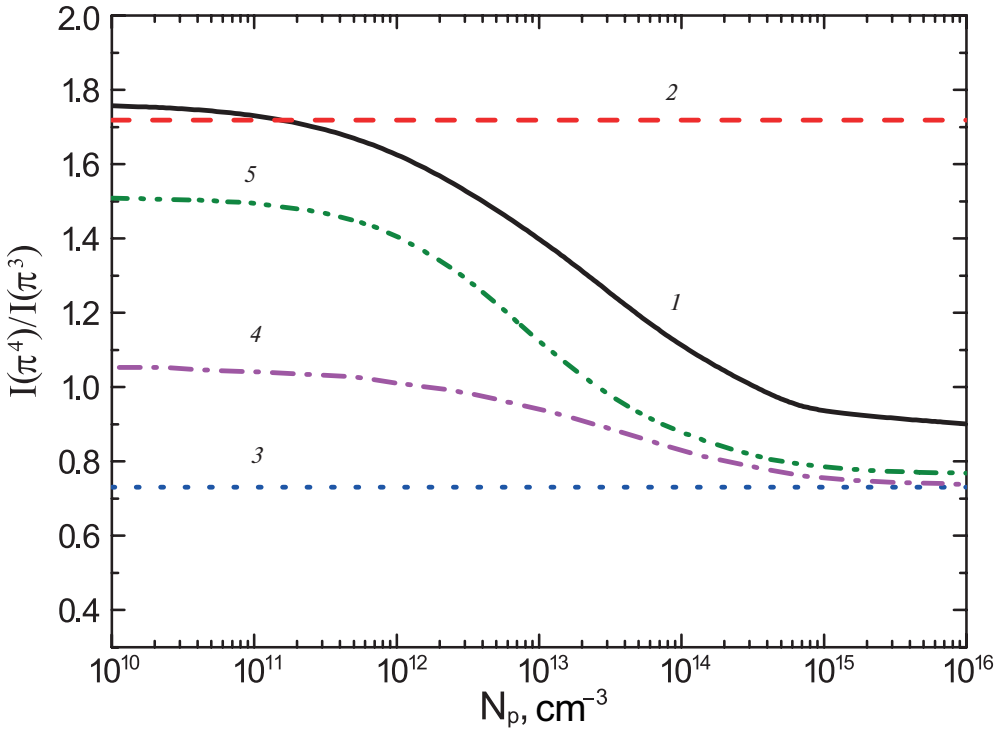

Fig. 13. The ratio of the intensities $I(\pi^4)$) / $I(\pi^3)$ of the H_α line depending on the plasma density (B = 5 T, E = 100 keV): *1* — calculated data for (9) with account of ionization; *2* — dynamic limit (11); *3* — statistical limit (10); *4* — data [17]; *5* — data from [19]

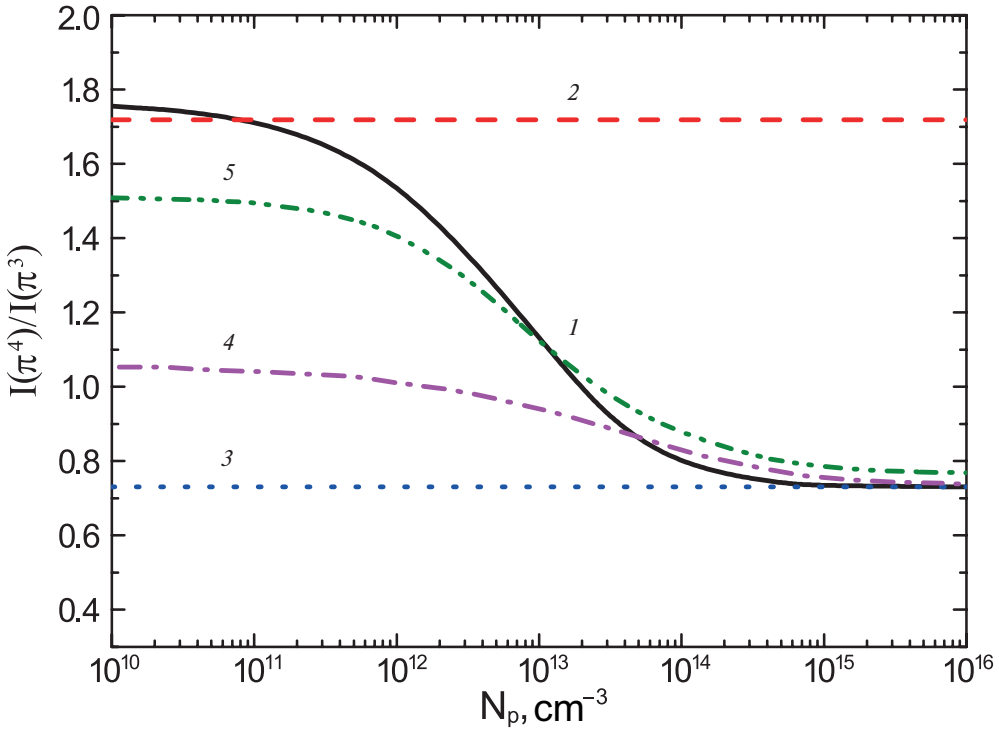

Fig. 14. The ratio of the intensities $I(\pi^4)$ / $I(\pi^3)$ of the H_α depending on the plasma density (B = 5 T, E = 100 keV): *1* — calculated data without (9) account of ionization; *2* — dynamic limit (11); *3* — statistical limit (10); *4* — data [17]; *5* — data from [19]

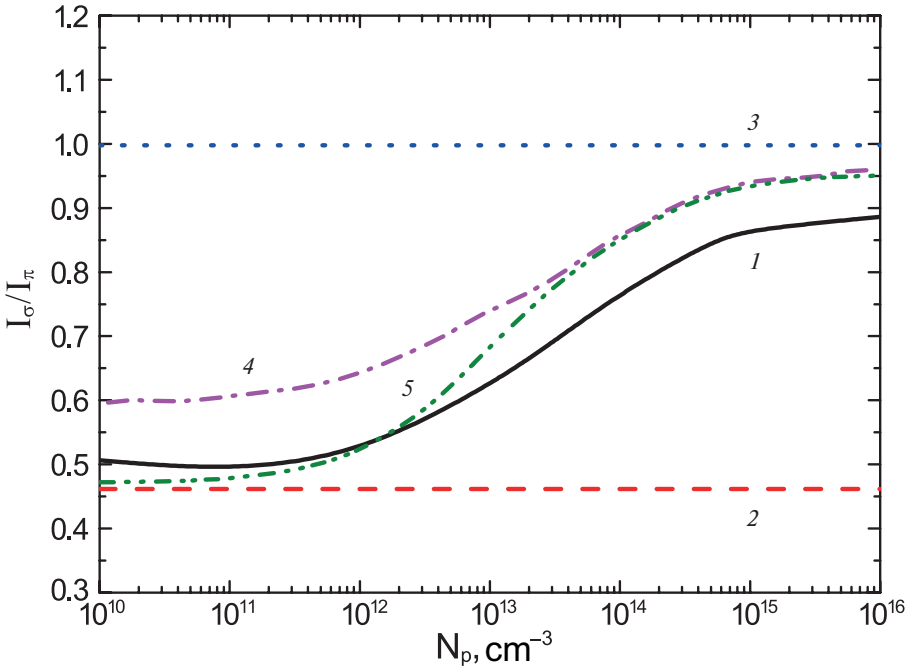

Fig. 15. The ratio of the σ-components intensities sum, divided by statistical weight, equal to 2 due to two independent polarizations, I_σ to the π-components intensities sum I_π of H_α line, depending on the plasma density ($B = 5$ T, $E = 100$ keV): *1* — calculated data for (9) with account of ionization; *2* — dynamic limit (11); *3* — statistical limit (10); *4* — data [17]; *5* — data from [19]

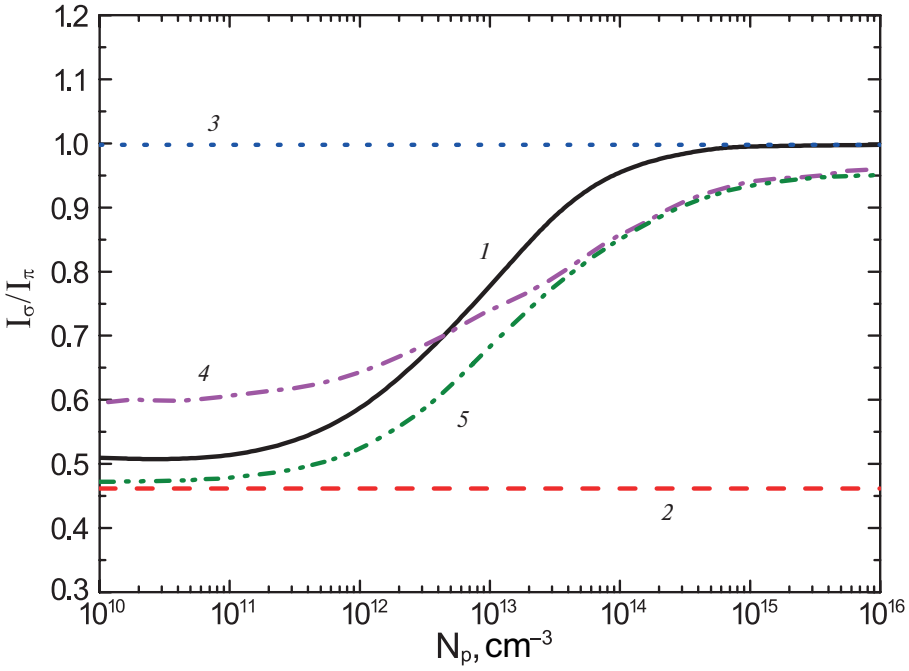

Fig. 16. The ratio of the σ-components intensities sum, divided by statistical weight, equal to 2 due to two independent polarizations, I_σ to the π-components intensities sum I_π of H_α, depending on the plasma density ($B = 5$ T, $E = 100$ keV): *1* — calculated data without (9) account of ionization; *2* — dynamic limit (11); *3* — statistical limit (10); *4* — data [17]; *5* — data from [19]

5. LIMITING CASES OF INTENSITY RATIOS

Fig. 11-16 show the ratios of intensities of some components of the H_α line as a function of plasma density. It can be seen from the figures that at low plasma densities, a coronal equilibrium is realized, and the ratio of intensities is close to the dynamic limit, and in the limit of higher densities, the ratio of intensities is close to the statistical limit. Deviation from it is associated with the ionization of the beam atoms in collisions with plasma protons. A comparison is made with the results of [17] and [19], in which spherical wave functions were used for the calculation of excitation cross sections with subsequent transition to a parabolic basis, and the cross sections themselves were calculated by the Glauber method. In [17], states up to $n = 10$, were considered in the kinetic model, while in [19] calculations were limited to states with $n = 5$. It is possible to notice the influence of the taken into account states number on the ratio of component intensities.

6. POLARIZATION CHARACTERISTICS OF MSE EMISSION SPECTRA

If the installation construction allows observation in a direction perpendicular to the beam velocity, the observation line forms an angle θ with the electric field direction. Then the oscillation vector of the electric field of the electromagnetic wave (EMW) radiation will be at an angle of $\pi / 2 - \theta$ to the direction of the electric field. The oscillation vector of the radiation of the π-components along the electric field will have a projection onto the EMW polarization vector, proportional to $\cos(\pi / 2 - \theta) = \sin\theta$. At the same time, the oscillation vector of the σ-component in the plane, perpendicular to the velocity, will form an angle of θ with the EMW polarization vector and contribute to the intensity $I_\sigma \cos^2\theta$, where I_σ denotes half the total intensity of the σ-components of the line. Also, the σ-components will contribute to the polarization of the EMF perpendicular to the plane formed by the electric field vector and the direction of observation, and directed along the velocity with an intensity equal to I_σ. Then the degree of polarization of the radiation relative to the direction of velocity under such an observation can be expressed as

$$P = \frac{I_\parallel - I_\perp}{I_\parallel + I_\perp} = \frac{I_\pi \sin^2\theta + I_\sigma \cos^2\theta - I_\sigma}{I_\pi \sin^2\theta + I_\sigma(\cos^2\theta + 1)} = \frac{(I_\pi - I_\sigma)\sin^2\theta}{I_\pi \sin^2\theta + I_\sigma(\cos^2\theta + 1)}. \quad (12)$$

It is important to note that in the limit of large densities and in the absence of ionization, the degree of polarization tends to zero at any angle of observation in the statistical limit. Figure 17 shows the dependences of the degree of polarization of the radiation of the H_α on angle θ at different plasma densities obtained within the framework of this kinetic model without account of proton ionization.

As can be seen in Fig. 17, with an increase in plasma density, the degree of polarization of the H_α line decreases to zero at any value of angle θ. At the same time, as noted in section. 3, accounting for ionization violates the statistical limit, and therefore, even at a high density, the degree of polarization does not tend to zero, as can be seen in Fig. 18. It is also interesting to follow the behavior of the degree of polarization at a fixed observation angle depending on the plasma density. These dependencies are shown in Fig. 19 and 20.

7. CONCLUSION

The polarization characteristics of the emission spectrum of the Stark components of the H_α line were studied under observation conditions perpendicular to the direction of the diagnostic beam of neutrals for MSE diagnostics injected across the magnetic field of the installation. To obtain a synthetic spectrum, a method has been developed for calculating the effective excitation cross sections of transitions between Stark sublevels of a hydrogen-like atom in collisions with protons, based on the Born method with a normalized transition probability and an adiabatic factor, which ensures more correct behavior of effective cross sections in the region of low collision energies when formally the applicability of the Born method is violated. The calculations were carried out in the basis of parabolic wave functions with a quantization axis along the direction of the electrodynamic electric field in the diagnostic beam rest frame. As in the Glauber method [11, 31, 32], it is taken into account that in this region of collision energies of heavy particles [11], characteristic of neutral beams of the

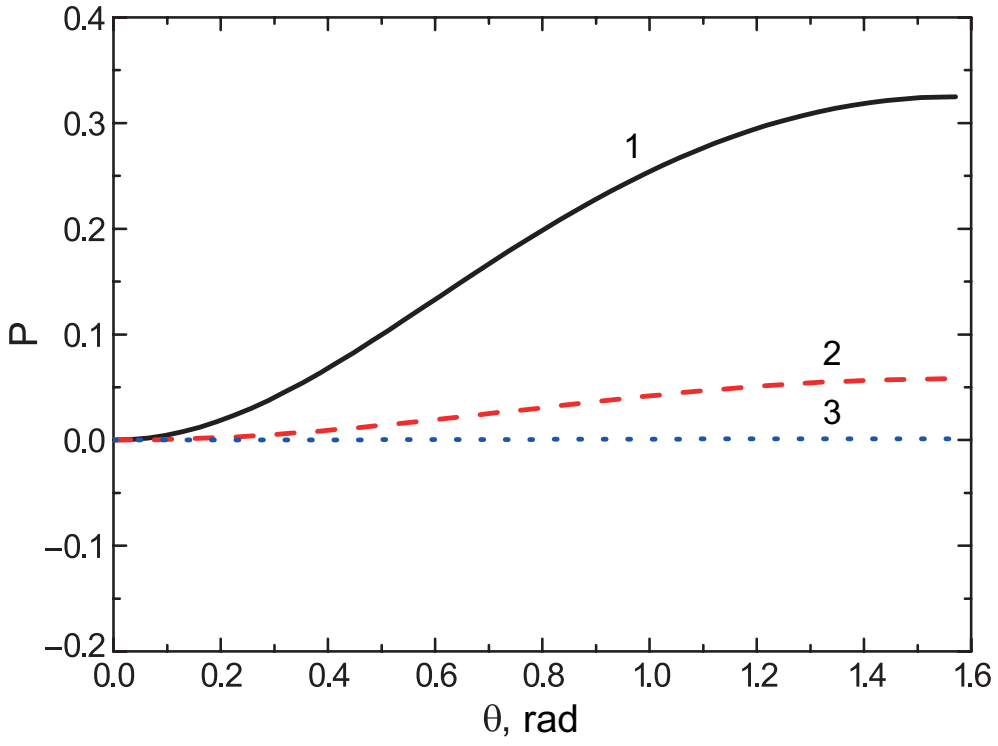

Fig. 17. The degree of polarization of the line H_α without account of the ionization effect, depending on the angle θ ($B = 5$ T, $E = 100$ keV) at different plasma densities N_e [cm^{-3}]: *1* — 10^{10}; *2* — $3 \cdot 10^{13}$; *3* — 10^{16}

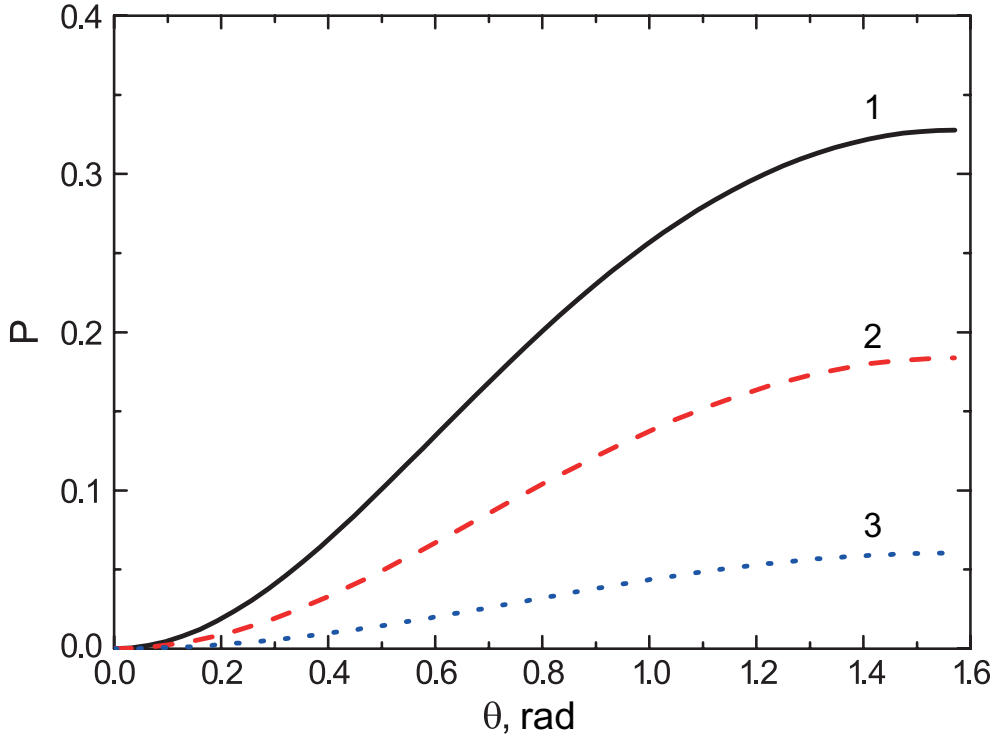

Fig. 18. The degree of polarization of the line H_α with account of the ionization effect, depending on the angle θ ($B = 5$ T, $E = 100$ keV) at different plasma densities N_e [cm^{-3}]: *1* — 10^{10}; *2* — $3 \cdot 10^{13}$; *3* — 10^{16}

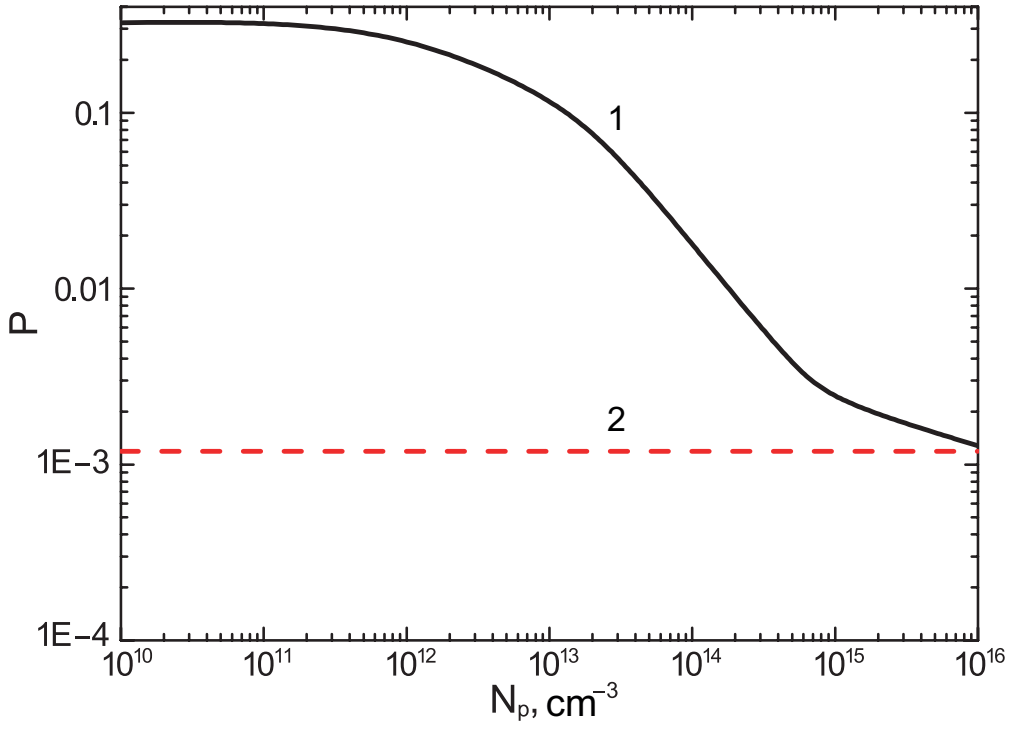

Fig. 19. The degree of polarization of the line H_α at $B = 5$ T, $E = 100$ keV, $\theta = 90^\circ$: *1* — without account of ionization depending on the plasma density; 2 – statistical limit in these conditions

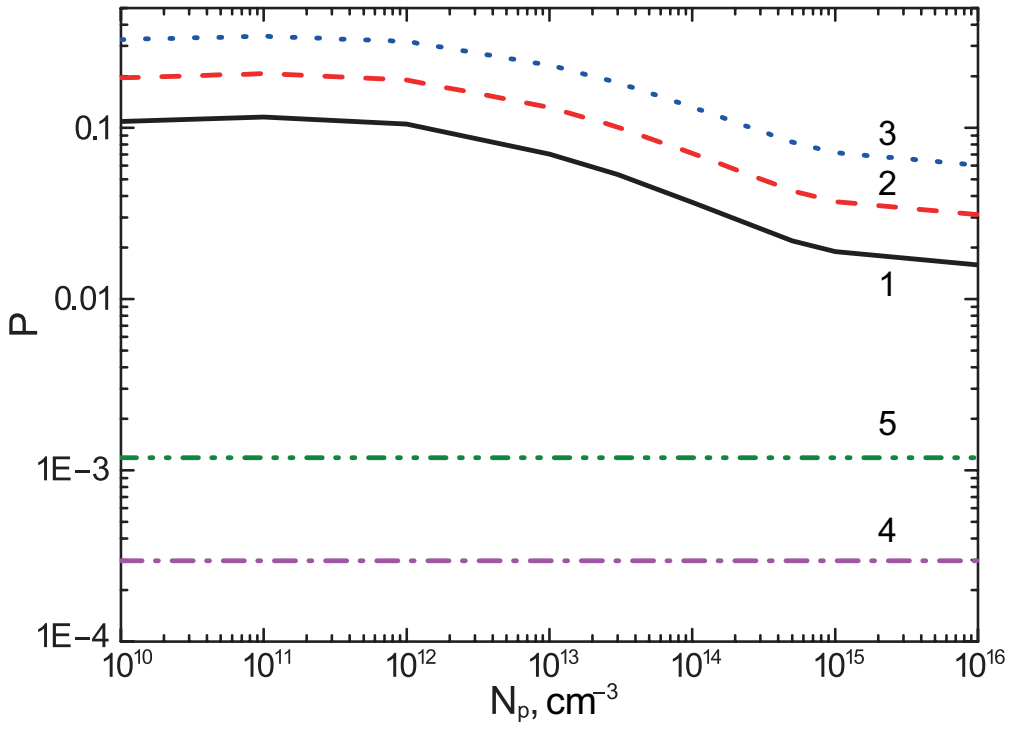

Fig. 20. The degree of polarization of the line H_α with account of the ionization effect, depending on the plasma density at various angles ($B = 5$ T, $E = 100$ keV): *1* — $\theta = 30^\circ$; *2* — $\theta = 45^\circ$; *3* — $\theta = 90^\circ$; *4* — statistical limit at $\theta = 90^\circ$; *5* — statistical limit at $\theta = 30^\circ$

MSE diagnostics, the effective transmitted momentum is perpendicular to the direction of the beam velocity. The kinetic collisional-radiative model has been elaborated for calculating the populations of Stark sublevels of a neutral atom in the basis of parabolic wave functions with quantum numbers n_1n_2m, covering all states with the principal quantum number n in the range 1-6. The populations of the Stark sublevels for n = 1-6, with and without account of collisional ionization by protons, and on their basis synthetic emission spectra of the intensity of the Stark components of the H_α line for different plasma and diagnostic beam parameters have been calculated. It has been shown that at low plasma density, the distribution of populations over Stark sublevels corresponds to coronal equilibrium. With an increase in plasma density, the nonthermodynamic nature of the equilibrium is preserved, in which the Stark sublevels populations are mainly determined by the processes of excitation and ionization in collisions with protons. Thus, in contrast to previous studies, the reasons for the nonthermodynamic character of the populations of Stark sublevels of neutral atoms of an energetic beam in a thermonuclear plasma with magnetic confinement have been analyzed and found. The behavior of the intensity ratio of the individual Stark components is studied depending on the plasma density and the parameters of the diagnostic beam within the statistical and dynamic levels population. The dependences of the polarization characteristic of the H_α line on the plasma density and observation angles relative to the direction of the induced electric field across the beam velocity are traced. A change in the statistical limit of the polarization characteristic under the influence of the proton ionization process for different observation angles relative to the direction of the induced electric field was revealed. All stages of the study are accompanied by a comparison with the literature data, which demonstrates a reasonable correspondence with the results of this work.

It should be emphasized that the previous calculations [17, 19], performed using cross sections calculated in the *nlm* basis of spherical wave functions, were mainly aimed at using already available data, although a verified database of excitation cross sections of hydrogen levels still does not exist. The entire set of cross sestions and rate coefficients presented and used in this work is calculated in a fairly universal way in the parabolic basis of wave functions for the first time in accordance with the physical formulation of the problem. At the same time, although there is some difference in kinetic calculations, their relative and qualitative behavior demonstrates similarity, which generally confirms the accuracy and reliability of the results of this work.

The results obtained are of general scientific interest and can be used for planning and interpreting experimental measurements aimed at determining the slope profile of the magnetic field line [1-7], which, in turn, allows to establish spatial distributions of the absolute values of the discharge parameters [3], for example, such as the cord stability factor [3], the discharge current [1-7] and the current density profile in the tokamak discharge [1-7].

ACKNOWLEDGEMENTS

The authors are grateful to I. A. Krupin, A. B. Kukushkin, V. A. Neverov, I. A. Zemtsov, M. R. Nurgaliev and E. Stambulchik for the useful discussions, as well as to A. Yu. Letunov for his active participation at the initial stage of the work.

FUNDING

This work was carried out within the framework of the state assignment of the National Research Center (NRC) Kurchatov Institute**.**

REFERENCES

1. Yu. I. Galushkin, Soviet Astronomy AJ 14, 301 (1970).

2. F.M. Levinton, R. J. Fonck, G. M. Gammel et al., Phys.Rev.Lett. 63, 2060 (1989).

3. V.A. Krupin, S. N. Ivanov, A. A. Medvedev et al, Preprint IAE–5940/7 (1995).

4. H.Y.-H. Yuh, PhD Thesis, MIT, Cambridge (2005).

5. R.Reimer, PhD Thesis, Universitat Greifswald, Greifswald (2016).

6. A. Thorman, PhD Thesis, The Australian National University, Canberra (2018).

7. F.M. Levinton and H. Yuh, Rev. Sci. Instrum. 79, 10F522 (2008).

8. M. F. Gu, C. T. Holcomb, R. J. Jayakuma et al., J. Phys.B: Atom. Mol.Opt.Phys. 41, 095701 (2008).

9. W. Mandl, R. C. Wolf, M. G. von Hellermann et al., Plasma Phys.Control. Fusion 35, 1373 (1993).

10. N.A. Pablant, K. H. Burrell, R. J. Groebner et al., Rev. Sci. Instrum. 79, 10F517 (2008).

11. O. Marchuk, Yu. Ralchenko, R. K. Janev et al., J. Phys.B: Atom. Mol.Opt.Phys. 43, 011002 (2010).

12. R. Reimer, A. Dinklage, J. Geiger et al., ASDEX Upgrade and Wendelstein 7-X Teams, Contrib.Plasma Phys. 50, 731 (2010).

13. E. Delabie, M. Brix, C. Giroud et al., Plasma Phys. Control. Fusion 52 125008 (2010).

14. A. Dinklage, R. Reimer, R. Wolf, Wendelstein 7-X Team, M. Reich, and ASDEX Upgrade Team, Fusion Sci.Technol. 59, 406 (2011).

15. R. Reimer, A. Dinklage, R. Fischer et al., and ASDEX Upgrade, Rev. Sci. Instrum. 84, 113503 (2013).

16. R.C. Wolf, A. Bock, O. P. Ford et al., J. Instrum. 10, P1008 (2015).

17. Yu. Ralchenko, O. Marchuk, W. Biel et al., Rev. Sci Instrum. 83, 10D504 (2012).

18. O. Marchuk, Yu. Ralchenko, and D.R. Schultz, Plasma Phys.Control. Fusion 54, 095010 (2012).

19. M. von Hellermann, M. de Bock, O. Marchuk et al., Atoms 7, 30 (2019).

20. O. Marchuk, D. R. Schultz, and Yu. Ralchenko, Atoms 8, 8 (2020).

21. I.I. Sobel'man, Introduction to the Theory of Atomic Spectra, Pergamon Press, Oxford (1972).

22. J.T. Park, J. E. Aldag, J. M. George et al., Phys. Rev.A 14, 608 (1976).

23. D. Rapp and D. Dinwiddie, Convergence of the Hydrogenic Expansion in H+−H Scattering, J. Chem. Phys. 57, 4919 (1972)

24. D.R. Bates and G. Griffing, Proc. Phys. Soc.A London 66, 64 (1953).

25. L.D. Landau, E. M. Lifshitz, Quantum Mechanics. Non-relativistic Theory, vol. III, 3d ed., Pergamon Press, 1991

26. I.S. Gradshteyn, I. M. Ryzhik, Table of Integrals, Series and Products, 8 th ed., Academic Press, Oxford (2015).

27. H. Bethe, E. Salpeter, Quantum Mechanics of One – and Two- Electron Atoms, Springer, Berlin (1957)

28. I.Y. Skobelev and A.V. Vinogradov, J. Phys.B: Atom. Mol. Phys. 11, 2899 (1978).

29. A.V. Vinogradov, I. Y. Skobelev A. M. Urnov et al, Proc. (Trudy) P.N. Lebedev Physics Institute 119, 120 (1980) (in Russian).

30. A.V. Vinogradov, Proc. P.N. Lebedev Physical Institute 51, Consultants Bureau, New York (1971) p. 45.

31. R. J. Glauber, High Energy Collision Theory, in Lectures in Theoretical Physics, Vol. 1, Interscience, New York (1959), p. 315.

32. V. Franco and B.K. Thomas, Phys.Rev.A 4, 945 (1971).

33. R.K. Janev, D. Reiter, and U. Samm, Collision Processes in Low-Temperature Hydrogen Plasmas, Forschungszentrum J¨ulich (2003).

34. R.K. Janev and J. J. Smith, Cross Sections for Collisions Processes of Hydrogen Atoms with Electrons, Protons and Multiply Charged Ions, Suppl.Nucl. Fusion 4, IAEA, Vienna (1993).

35. R.E. Olson, J. Phys.B 13, 483 (1980).

36. R. J. Damburg and V.V. Kolosov, J. Phys.B: Atom. Mol. Phys. 12, 2637 (1979).

37. P.A. Braun and E.A. Solov'ev, J. Phys.B: Atom. Mol. Phys. 17, L211 (1984)